Study of hydrogen Stark profiles by means of computer simulation

R. Stamm* and E. W. Smith
National Bureau of Standards, Boulder, Colorado 80302

B. Talin
Département de Physique des Interactions Ioniques et Moléculaires
(Equipe de Recherche No. 898 du Centre National de la Recherche Scientifique),
Université de Provence, Centre de Sainte Jérôme, F-13397 Marseille Cédex 13, France
(Received 21 October 1983)

A computer simulation technique is used to calculate hydrogen spectral lines emitted by a plasma. These calculations are used to study ion dynamic effects on the line profiles. Results are obtained for Lyman-α, Lyman-β, and Lyman-γ lines, and comparisons are made with experimental results and with other theoretical methods.

I. INTRODUCTION

Recent measurements[1,2] of the Stark profiles of the hydrogen Lyman-α and -β lines in an arc plasma have revealed a sizeable discrepancy between theoretical[3,4] and experimental results. The observed half-width of the L_α line is almost twice as large as the theoretical value from Refs. 3 and 4 at an electron temperature of 10^4 K and an electron density of 10^{17} cm^{-3}; the observed dip in L_β is about one-third of the theoretical value for the same plasma conditions. These discrepancies are considerably larger than similar results observed[5,6] for the Balmer series. From various experimental[6] and theoretical[7–9] analyses, it has been concluded that the main reason for these discrepancies is probably the static ion approximation used in Refs. 3 and 4. Unfortunately it has been very difficult to correct this approximation because, for electron densities of experimental interest (e.g., $N_e > 10^{14}$ cm^{-3}), the ion dynamic effects are characterized by overlapping strong collisions and this prevents the use of the familiar binary collision theories, such as the unified theory.[10,11] Several approximate methods have been proposed for small ion dynamic corrections and for moderate densities, e.g., 10^{17} cm^{-3}; these approaches provide some improvement but they still disagree with the experimental data and with one another. A new formalism proposed by Greene[12] shows some promise and the model microfield method (MMM) proposed by Brissaud and Frisch[13] and developed by Seidel[14] has already had considerable success in treating strong ion dynamic effects. In this paper, we present yet another approach to the treatment of strong ion dynamic effects, namely, the method of computer simulation.

In the present approach, the ions are represented by a computer model and the electrons are treated by a time-ordered impact theory, as will be discussed in Secs. II and III. The results of this approach are compared with experimental data as well as other theoretical approaches, particularly the MMM and the new formalism of Greene. The analysis presented in this paper concentrates mainly on the L_α and L_β lines because the ion dynamic effects are quite large for these lines and one avoids the computationally annoying and expensive problems of the large atomic matrices involved in Balmer line calculations.

II. SEPARATION OF ELECTRON AND ION EFFECTS

In this section we will briefly outline the assumptions of our basic model for the plasma; since most of these are well known, we will not spend a great deal of time discussing their validity. This is done primarily to emphasize the fact that computer simulation does not avoid all of the problems of plasma physics.

We will assume first that the plasma may be regarded as a collection of statistically independent shielded electrons and ions sometimes called quasiparticles. That is, these fictitious electrons and ions move in straight lines and they produce Debye-shielded electric fields

$$\epsilon_s(r) = (e/r^2)(1 + r/\lambda_D)\exp(-r/\lambda_D) , \tag{1}$$

where λ_D is the Debye-shielding length. This model does not include the so-called dynamic shielding effects which are important in nonthermal plasmas,[15,16] nor does it properly account for some ion-ion and electron-ion correlation[17] effects which are important for very high electron densities.

The line shape for the Lyman series is given by the Fourier transform of an atomic dipole autocorrelation function which may be expressed as

$$\langle \vec{d}(t)\cdot\vec{d}(0)\rangle = \sum_{a,a',b} \{U_{aa'}(t)\}_{\rm av}\vec{d}_{a'b}\cdot\vec{d}_{ba}\rho_a e^{-i\omega_{ab}t} , \tag{2}$$

where $\vec{d}$ is the dipole operator for a hydrogen atom, a and a' are the excited states for the particular Lyman line of interest, b is the hydrogen ground state, ρ_a is the density matrix or statistical weight factor for the excited states, $\omega_{ab} = (E_a - E_b)/\hbar$ where E_a and E_b are the energies of the excited and ground states, $U(t)$ is the time development operator for a hydrogen atom in the presence of the electric field produced by the electrons and ions, and the average, denoted by $\{\ \}_{\rm av}$, is an average over all possible

time histories and initial field strengths for this electric field (e.g., an average over all initial positions and velocities for the electrons and ions). In this equation we have neglected inelastic collisions; that is, we do not consider matrix elements of $U(t)$ between states having different principal quantum numbers. The time development operator satisfies the Schrödinger equation

$$i\hbar\frac{\partial}{\partial t}U(t)=[V_e(t)+V_i(t)]U(t)\ , \tag{3}$$

$$V_e(t)=e^{itH_0/\hbar}\vec{d}\cdot\vec{\epsilon}_e(t)e^{-itH_0/\hbar}\ , \tag{4}$$

$$V_i(t)=e^{itH_0/\hbar}\vec{d}\cdot\vec{\epsilon}_i(t)e^{-itH_0/\hbar}\ , \tag{5}$$

where H_0 is the Hamiltonian for an unperturbed hydrogen atom while $\vec{\epsilon}_e(t)$ and $\vec{\epsilon}_i(t)$ are the electric fields at the atom generated by the electrons and ions, respectively. The formal solution to Eq. (3) is

$$U(t)=\mathcal{O}\exp\left[-(i/\hbar)\int_0^t[V_e(s)+V_i(s)]ds\right]\ , \tag{6}$$

where $\mathcal{O}$ is the time-ordering operator.

Since we choose to use an impact theory for the electrons and a computer simulation for the ions, it is necessary to separate their respective contributions to $U(t)$. We do this by defining electron and ion terms

$$U_e(t)=\mathcal{O}\exp\left[-(i/\hbar)\int_0^t V_e(s)ds\right]\ , \tag{7}$$

$$U_i(t)=\mathcal{O}\exp\left[-(i/\hbar)\int_0^t V_i(s)ds\right] \tag{8}$$

so that Eq. (6) may be written

$$U(t)=\mathcal{O}U_i(t)\mathcal{O}\exp\left[-(i/\hbar)\int_0^t U_i^\dagger(s)V_e(s)U_i(s)ds\right]\ , \tag{9}$$

which may be verified by differentiating with respect to t and comparing with Eq. (3).

The ion operators $U_i(s)$ will be neglected where they appear in the electron operator; that is, Eq. (9) will be approximated by

$$U(t)=\mathcal{O}U_i(t)U_e(t)\ . \tag{10}$$

To justify this approximation, we note that the ion field may be regarded as essentially constant during an electron collision, hence the $U_i(s)$ operators have the effect of a static Stark shift of the hydrogenic energy levels. This Stark shift, the order of $\Delta E=e(Z_a-Z_{a'})\epsilon_i$ where Z is the Z component of $\vec{d}$, will produce a modulation of the electron interaction of the form $V_e(s)\exp(is\,\Delta E/\hbar)$. Since $V_e(t)$ is nonzero only for a time on the order of $T_e=1/\omega_{pe}$ where ω_{pe} is the electron plasma frequency, this modulation will be important only when $\Delta E/\hbar\omega_{pe}\geq 1$. For L_β, Z_a-Z_a' is estimated by $27a_0/2$ where a_0 is the Bohr radius, ϵ_i is estimated by e/r_0^2 where r_0 is the average ion separation, and $4\pi r_0^3/3=N_e^{-1}$; such an estimate indicates that this ion field modulation effect should be negligible for $N_e\leq 1/(100a_0)^3=6.7\times10^{18}$ cm^{-3}. Such ion field exponentials are sometimes treated by a cutoff procedure.[18]

We will make an additional approximation by ignoring the time-ordering operator in Eq. (10) and using

$$U(t)=U_i(t)U_e(t)\ . \tag{11}$$

This does not completely ignore time ordering because both U_i and U_e are time ordered [see Eqs. (7) and (8)]. The time ordering ignored in Eq. (11) is that which entangles electron collisions with ion collisions. By analogy with other time-ordering effects,[19] this is expected to produce errors on the order of 5% or less in the half-width.

Since the electrons and ions are assumed to be statistically independent, their averages may be performed separately and Eq. (2) reduces to

$$\langle\vec{d}(t)\cdot\vec{d}(0)\rangle=\sum_{a,a',a'',b}[\{U_i\}_{\rm av}]_{aa''}(e^{-\Phi_e t})_{a''a'}\times\vec{d}_{a'b}\cdot\vec{d}_{ba}\rho_a e^{-i\omega ab^t}\ , \tag{12}$$

where the averaged electron operator $\{U_e\}_{\rm av}$ was replaced by $\exp(-\Phi_e t)$ which is the result obtained by an impact theory for the electrons. In our calculations, Φ_e is obtained by taking the impact limit of a time-ordered unified theory calculation performed by Greene.[12,20] The ion operator $\{U_i\}_{\rm av}$ is evaluated by the computer simulation technique discussed in Sec. III.

III. COMPUTER SIMULATION FOR THE IONS

A primary consideration of the ion dynamics problem is the effect of radiator motion. Seidel[21] has shown that a plasma appears anisotropic to a moving atom and one finds two different Stark profiles $I^{\|}$ and $I^{\perp}$ corresponding to emission parallel to and perpendicular to the direction of radiator motion. For the L_β line this effect has been shown to be negligible after the average over radiator velocities is performed[22] and the usual Doppler convolution procedure is adequate provided that the effective mass of the ion is taken to be the reduced mass for a radiator-perturber pair.

We therefore employ the computer simulation technique developed in the two previous papers.[23,24] In that procedure, N ions are randomly distributed in a sphere of radius R, N velocity vectors are chosen at random (weighted by a Maxwellian probability distribution), the ions are allowed to move on straight paths, and the Debye-shielded electric field produced at the center of the sphere is calculated as a function of time. The procedure for reinjecting ions which leave the sphere was discussed in Ref. 23 and it was observed that this simulation procedure produces the correct static electric field distribution and the correct electric field autocorrelation function. To apply this simulation procedure to line broadening we imagine that the radiating atom is stationary at the center of the sphere and the ion mass used in the calculation is the reduced mass for an atom-ion pair as noted above.

The radius of the sphere was given by Eq. (1.1) of Ref. 23 as $4\pi R^3/3=N/N_e$, where N is the number of ions in the simulation and N_e is the density of the plasma we wish to model. In this paper, all calculations were performed with $N=125$ ions so that $R=3.10/N_e^{1/3}$. For low plasma densities N_e the sphere radius R becomes larger; however, the Debye length $\lambda_D=(kT/4\pi N_e e^2)^{1/2}$ increases more rapidly than R as N_e decreases. Since the

simulation neglects ions outside the sphere of radius R, we must insure that these ions are truly negligible by requiring $R \gg \lambda_D$. This means that our calculations with a fixed $N=125$ will not be valid for some low densities. For an electron temperature of $T=10^4$ K, we have $\lambda_D=R$ at $N_e=1.2\times10^{14}$ cm^{-3}; consequently, we have restricted our calculations to $N_e \geq 10^{15}$ cm^{-3}.

The ion operator $U_i(t)$ is obtained by numerically integrating the Schrödinger equation [see Eq. (8)]

$$i\hbar\frac{\partial}{\partial t}U_i(t)=V_i(t)U_i(t)\ , \tag{13}$$

where V_i is given by Eq. (5). This matrix equation is actually treated as n_q^2 coupled scalar equations (n_q is the principal quantum number for the excited state) in which the matrix elements of U_i and V_i are complex numbers. Several algorithms were tested and the best compromise between computer time and numerical precision or stability was found to be a Merson differential-equation solver which uses variable time steps.[25]

The ion average $\{U_i(t)\}_{\rm av}$ required by Eq. (12) is evaluated by randomly choosing several different initial configurations of ions, solving Eq. (13) for each of them, and then adding all of the $U_i(t)$ together for each value of t. In general, a large number of configurations are needed to keep the noise level low; for example, the data presented in Figs. 1 and 2 of Ref. 23 used 40 000 configurations. This would be impractical for our purposes here since we have to solve Eq. (13) for each configuration and the computer time required would be prohibitive. We have therefore used a "noise-reducing filter" which is based on the fact that the static electric field distribution function $P_{eq}(\epsilon)$ is known from previous theoretical work.[26]

To construct our noise-reducing filter, we first note that, for a total of N_c configurations, there should be $N_k=4\pi N_c\int_k P_{eq}(\epsilon)\epsilon^2 d\epsilon$ which have an initial field strength in the range $(\epsilon_k,\epsilon_k+\Delta\epsilon_k)$ where $\int_k$ denotes an integral over $(\epsilon_k,\epsilon_k+\Delta\epsilon_k)$. Theoretically, one should obtain this result for any N_c and any arbitrarily chosen values ϵ_k and $\Delta\epsilon_k$ but of course the computer simulation does not always give this result due to statistical fluctuations. These fluctuations are reduced as $1/\sqrt{N_c}$, and for large N_c, e.g., 40 000, the fluctuations are not a problem, but for N_c on the order of 1000 or less this statistical noise must be reduced. We have therefore divided the range of initial field strengths into 24 domains corresponding to 24 values of ϵ_k and $\Delta\epsilon_k$, and for a fixed N_c the set of 24 N_k are calculated as indicated above. The computer simulation is then constrained to give exactly this set of N_k. That is, ion configurations are generated at random, they are sorted according to their initial field strengths into one of the 24 domains, and, once the required number of configurations N_k has been found for some domain $(\epsilon_k,\epsilon_k+\Delta\epsilon_k)$ we reject any additional configurations which would fall into this domain. We continue generating configurations until all 24 domains are filled with the correct number of configurations. This procedure provides us with N_c configurations which are distributed in such a way that the N_k provide a histogram which closely approximates the known electric field distribution function $P_{eq}(\epsilon)$ for the initial field strength.

This noise filter greatly reduces the statistical noise for the initial configurations, but as time increases the ions move and after a time on the order of a few times $1/\omega_{\rm pi}$ (where $\omega_{\rm pi}$ is the ion plasma frequency) the noise level increases to the value it would have had without the noise filter. Nevertheless, this procedure significantly reduces the noise for correlation functions such as $\langle\vec{d}(t)\cdot\vec{d}(0)\rangle$, which is needed for line broadening, because the correlation functions are largest at $t=0$ where the noise reduction is greatest and they decrease with t as the noise is increasing. The calculations presented in this paper have used $N_c=1100$ configurations. The effect of the residual statistical noise (i.e., that remaining even after the noise filter is applied) was checked by performing line-shape calculations for several independent sets of 1100 ions. In this manner we found that the line-center intensity was calculated to better than $\pm2\%$ and the noise level reached $\pm3\%$ at about twice the half-width and $\pm10\%$ at 10 times the half-width. Even by going down to 220 configurations, we estimated the error bounds to be $\pm5\%$ at line center.

The Fourier transform of the dipole autocorrelation function was performed in only a few seconds using Filon's rule[27] and the line profile was obtained from

$$I(\omega)=\frac{1}{\pi}\,\mathrm{Re}\int_0^\infty \exp(-i\omega t)\langle\vec{d}(t)\cdot\vec{d}(0)\rangle\ . \tag{14}$$

A complete Lyman-β profile calculation, including the microfield simulation, required about 20 min of CPU time on a (CDC) Cyber-750 computer and most of this time was spent in solving the differential equation.

IV. RESULTS

Calculations have been performed for Lyman lines for various temperatures, densities, and ion masses in order to compare the results of the computer simulation technique with experimental data and with other theoretical approaches. Some of the line profile data are presented in terms of the parameter $\alpha=\Delta\lambda/F_0$ where $\Delta\lambda$ is the wavelength separation (in Å) from line center and $F_0=2.6eN_e^{2/3}=1.25\times10^{-9}N_e^{2/3}$.

In Fig. 1 we compare our calculations of the L_α, L_β,

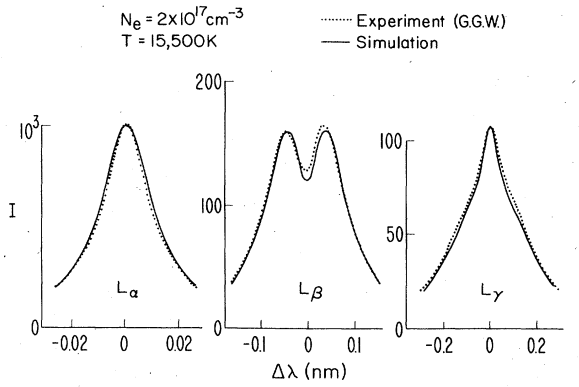

FIG. 1. Comparison of simulation calculations for H-Ar$^+$ with experimental results (Ref. 29).

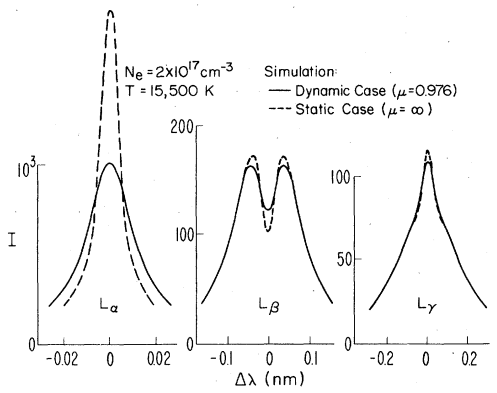

FIG. 2. Computer simulation results for static ions ($\mu \rightarrow \infty$) and dynamic ions for H-Ar$^+$ ($\mu = 0.976$).

and L_γ lines for H-Ar$^+$ with experimental data[28,29] at $N_e = 2\times 10^{17}$ cm^{-3} and $T = 15\,500$ K. The agreement is quite good although our calculations are 8% broader than the observed L_α profile and 6% narrower than the observed L_γ, and the calculated L_β dip is 20% deeper than is observed. These discrepancies are not too serious considering that the experimental accuracy is on the order of 5% and the effects which we have neglected (see Secs. II and III) are certainly on the order of 5% or 10%. In Fig. 2 we compare the same H-Ar$^+$ ($\mu = 0.976$) profiles with the results which would have been obtained for static ions ($\mu = \infty$). From this comparison we see that ion dynamic effects have increased the L_α half-width by a factor of 2.14 and the L_β dip is reduced from 0.41 to 0.25. The effect of ion dynamics on the L_α and L_β lines is therefore much greater than the 5% or 10% error level of the calculations. It is also clear from these data that the effect of ion dynamics is greatest for the L_α line, slightly less for L_β, and barely noticeable for L_γ.

To explain this decrease in ion dynamic effect for the higher series members, we first recall that the line shape is proportional to the Fourier transform of the dipole autocorrelation function, Eq. (2). For a given frequency difference $\Delta\omega_{ab} = \omega - \omega_{ab}$ the oscillating exponentials in this Fourier transform will strongly reduce the integral

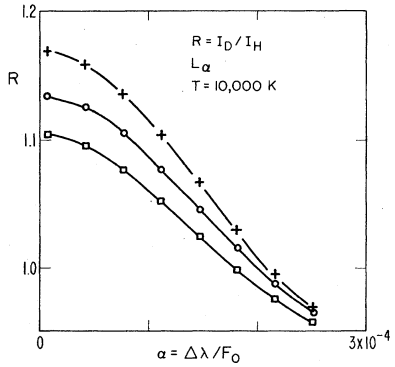

FIG. 3. Ratio $R = I_D/I_H$ of L_α profiles for deuterium (I_D) and hydrogen (I_H) emitters perturbed by Ar$^+$ for three densities: $N_e = 3\times 10^{16}$ cm^{-3} (crosses), 10^{17} cm^{-3} (circles), and 3×10^{17} cm^{-3} (squares).

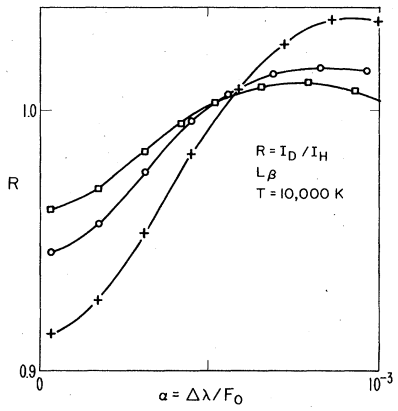

FIG. 4. Ratio $R = I_D/I_H$ of L_β profiles for deuterium (I_D) and hydrogen (I_H) emitters perturbed by Ar$^+$ for three densities: $N_e = 3\times 10^{16}$ cm^{-3} (crosses), 10^{17} cm^{-3} (circles), and 3×10^{17} cm^{-3} (squares).

for large values of t, hence one only needs to consider times shorter than $1/\Delta\omega_{ab}$. If the ions do not move appreciably during this time (i.e., if their interaction with the radiator is essentially constant) they may be regarded as static. Now the duration of a strong ion collision is well known as the inverse of the Weisskopf frequency, $\tau_w = 1/\Delta\omega_w$, hence the condition that the ions may be regarded as static is $\Delta\omega_{ab} \gg \Delta\omega_w$ [e.g., Sec. (2) of Ref. 30]. For the Lyman series, the Weisskopf frequency is $\Delta\omega_w = \hbar v^2/1.5 n_q^2 a_0 e^2$, where v is the average ion velocity (using the reduced mass), n_q is the principal quantum number for the excited state, and $a_0 = 5.29\times 10^{-9}$ cm is the Bohr radius. If the ion field is static, the excited state is split into $n_q + 1$ Stark components with a perturbation energy proportional to the electric quantum number[31] q which may take the values $0, \pm 1, \pm 2, \ldots, \pm(n_q - 1)$. The average Stark splitting for each of these components is $\omega_q = \frac{3}{2} n_q q a_0 e F_0/\hbar$, where F_0 is the average field strength $F_0 = e/r_0^2$ and $4\pi r_0^3/3 = 1/N_e$. Thus if one is interested in a frequency which is well separated from all of these Stark components, $\Delta\omega_q = |\omega - \omega_q| \gg \Delta\omega_w$, then the ions may be treated as static.

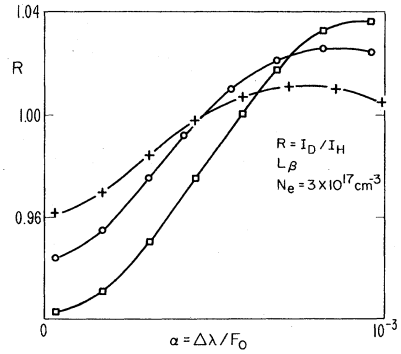

FIG. 5. Ratio of $R = I_D/I_H$ of L_β profiles for deuterium (I_D) and hydrogen (I_H) emitters perturbed by Ar$^+$ at three temperatures: $T = 10\,000$ K (crosses), 20 000 K (circles), and 40 000 K (squares).

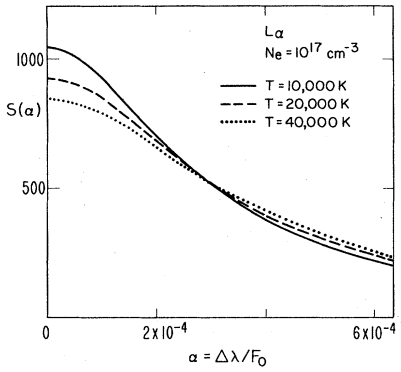

FIG. 6. Effect of temperature on L_α profile for H-Ar$^+$.

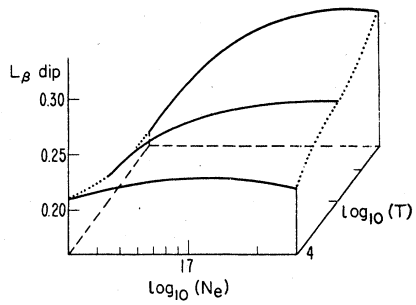

FIG. 8. Dip of L_β for H-Ar$^+$ as a function of $\log_{10}N_e$ and $\log_{10}T$ for 3×10^{16} cm$^{-3}\leq N_e\leq 3\times10^{17}$ cm^{-3} and 10^4 K$\leq T\leq 4\times10^4$ K.

For Lyman γ there are five Stark components, $q=0,\pm1,\pm2$, and, at an electron density of $N_e=2\times10^{17}$ cm^{-3}, the wavelength separation between these Stark components is $\Delta\lambda_s=0.05$ nm whereas the wavelength corresponding to the Weisskopf frequency $\Delta\omega_w$ at $T=15\,500$ K is $\Delta\lambda_w=0.001$ nm. Thus $\Delta\lambda_s/\Delta\lambda_w\sim50$ and the ions may be regarded as static over most of the Lyman-γ profile, and even at the center of a Stark component (e.g., at line center where the $q=0$ component lies) the static approximation is in error for only one component whereas the contribution from the other four components is calculated correctly. Thus for Lyman γ, the static ion approximation produces a relatively small error. For Lyman α at the same temperature and density, $\Delta\lambda_w=0.004$ nm while $\Delta\lambda_s=0.025$ nm, and there are only three Stark components. In this case $\Delta\lambda_s/\Delta\lambda_w=6$, hence one may not safely use the static ion approximation for any of the Stark components for wavelengths in the line-center region. In fact, it is particularly bad for the unshifted central Stark component.

It is also interesting to note that $\Delta\lambda_s$ increases with the density and $\Delta\lambda_w$ increases with increasing temperature. This means that, for a given line, the ion dynamic effect should become stronger for higher temperatures and it should become weaker for higher densities. This behavior is illustrated in Figs. 3–5 in which we have plotted the ratio $R=I_D/I_H$ of the profile I_D for D-Ar$^+$ and I_H for H-Ar$^+$; in these figures we have used the scaled wavelength parameter $\alpha=\Delta\lambda/F_0$. From the data in Figs. 3–5, it is clear that the ratio R approaches unity as the density increases and as the temperature decreases [cf. Fig. (6) of Ref. 28].

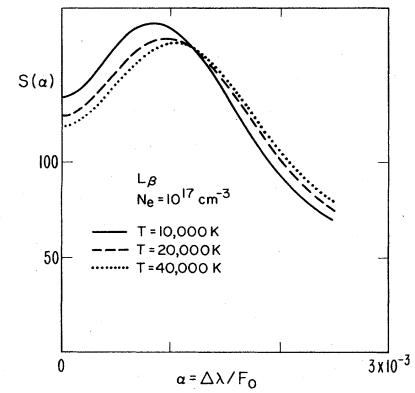

FIG. 7. Effect of temperature on L_β profile for H-Ar$^+$.

We have also compared computer simulation calculations of $R=I_D/I_H$ with experimental data[28] at $N_e=2\times10^{23}$ cm^{-3} and $T=15\,500$ K. In the center of L_α, the experimental profile, which includes Doppler broadening, gave $R=1.17$ whereas the value obtained by computer simulation was $R=1.16$. For L_β, which is not significantly affected by Doppler broadening, both experiment and simulation give $R=0.95$.

In Figs. 6 and 7 we have plotted the L_α profiles for three different temperatures. For L_α, an increase in temperature increases the broadening; increasing T from 10 000 to 20 000 K decreases the line-center intensity by 9% and increasing T from 20 000 to 40 000 K produces an additional 17% decrease.

For L_β an increase in temperature produces a decrease in both the line-center intensity and the peak intensity, thereby producing a distinct shift of the ion peak on the α scale. For an electron density of $N_e=10^{17}$ cm^{-3} the position of the peak shifts by 12% as T increases from 10 000

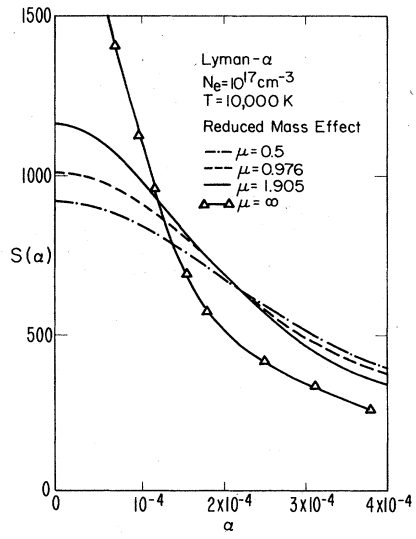

FIG. 9. Reduced mass effect on L_α. We have plotted profiles for H-H$^+$ ($\mu=0.5$), H-Ar$^+$ ($\mu=0.976$), D-Ar$^+$ ($\mu=1.905$), and the static ion case ($\mu=\infty$).

to 20000 K and by 20% as T goes to 40000 K. While this tendency for the shift is confirmed for all other densities calculated, no definite tendency is observed for the dip which is defined as $(I_{max}-I_{min})/I_{max}$, where I_{min} denotes the intensity at line center. In the density range investigated, the L_β dip sometimes increases (for $N_e=3\times10^{16}$ cm^{-3}) and sometimes decreases (for $N_e=3\times10^{17}$ cm^{-3}) with increasing temperature. This behavior of the L_β dip is illustrated in Fig. 8.

Finally, in Fig. 9 we have plotted the L_α profile at $N_e=10^{17}$ cm^{-3} and $T=10000$ K for several different values of the reduced mass. These profiles correspond to H-H$^+$ ($\mu=0.5$), H-Ar$^+$ ($\mu=0.976$), D-Ar$^+$ ($\mu=1.905$), and the $\mu\to\infty$ or static limit. As already noted, the H-Ar$^+$ and D-Ar$^+$ profiles agree with experimental data[28] and the general variation of the profile as a function of reduced mass also agrees with the results observed for the Balmer line H_α.

V. COMPARISON WITH OTHER ION DYNAMIC THEORIES

The comparisons presented in Sec. IV indicate that ion dynamics is responsible for essentially all of the difference between experimental data and the results of a static ion theory. In addition, the computer simulation has been able to successfully describe these ion dynamic effects and provide good agreement with experimental data. In this section we will compare the computer simulation results with two recent theoretical approaches which include ion dynamic effects.

Our first comparison is with a theoretical approach proposed by Greene[12] in which electric fields are evaluated by following ion trajectories as in an impact or unified theory, and the overlap of simultaneous strong collisions is included in an approximate manner. This comparison is interesting because we use the same electron collision operator and thus have identical line shapes in the static ion limit. Figures 10 and 11 show, for a density of 10^{17} cm^{-3} and a temperature of 10^4 K, that our simulation predicts a significantly stronger effect of ion dynamics than the calculation by Greene. Going from the static to the dynamic ion case, the intensity for L_α is reduced by a factor of 1.85 in the simulation, whereas the profile of Ref. 12 is lower only by a factor of 1.45. For L_β the dip is reduced from 0.41 to 0.22 in the simulation and only from 0.41 to 0.29 in Ref. 12. These differences are probably related to the approximations made in Ref. 12 for the evaluation of the ionic collision operator.

In Ref. 12 this operator was evaluated by assuming that

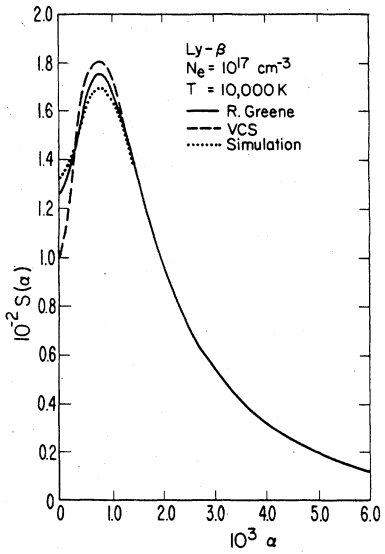

FIG. 11. Comparison of computer simulation with calculations of Greene (Ref. 12) and VCS (Ref. 4) (static ion) results for the L_β line of H-Ar$^+$.

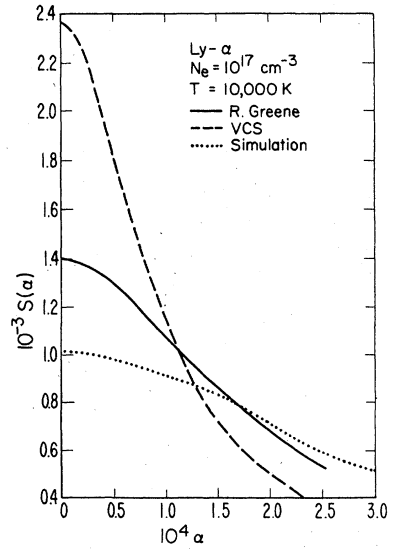

FIG. 10. Comparison of computer simulation with calculations of Greene (Ref. 12) and VCS (Ref. 4) (static ion) results for the L_α line of H-Ar$^+$.

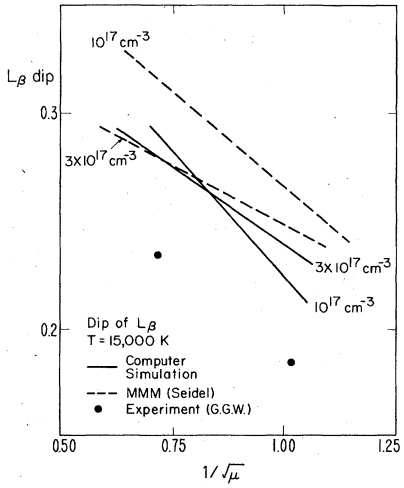

FIG. 12. L_β dip as a function of the reduced mass μ for a fixed temperature $T=15000$ K. Theoretical MMM curves (Ref. 32) and simulation results are plotted for the two densities $N_e=10^{17}$ cm^{-3} and $N_e=3\times10^{17}$ cm^{-3}. No change of the dip has been observed experimentally in this density range by GGW (Ref. 28).

the atomic dipole always points in the direction of the electric field [see Eqs. (22)—(26) of Ref. 12]. In Ref. 9 it was shown that this adiabatic approximation can lead to errors the order of 30% in the half-width, hence this approximation may be the reason for discrepancies between the computer simulation results and the calculations of Ref. 12.

In the light of the success of the MMM in describing Stark profiles it is also desirable to make comparisons with that method. In Fig. 12 we have compared MMM results with the computer simulation for the dip in L_β. This dip was measured by Geisler, Grützmacher, and Wende[28] (GGW) for D-Ar$^+$ ($1/\sqrt{\mu}=0.72$) and H-Ar$^+$ ($1/\sqrt{\mu}=1.01$) [see Fig. (7) of Ref. 28] and they found that there was no observable change in the dip as a function of density when $T=15\,000$ K. In Fig. 12 it is clear that the MMM predicts an observable density dependence for these two values of reduced mass whereas the simulation predicts a very weak density dependence more in agreement with the measurements. The MMM can be brought into closer agreement with the simulation by using the same electron collision operator.[32] For example, for a density of $N_e=10^{17}$ cm^{-3} and a temperature $T=10^4$ K, the L_α dip changes from 0.39 at $\mu=\infty$ to 0.25 at $\mu=0.976$ (H-Ar$^+$) when using the full MMM (i.e., the MMM applied to both electrons and ions). If the MMM is applied only to the ions while an impact theory with Greene's collision operator is used for the electrons, the L_β dip changes from 0.42 at $\mu=\infty$ to 0.25 at $\mu=0.976$. The latter is closer to the simulation which goes from 0.42 at $\mu=\infty$ to 0.23 at $\mu=0.97$.

For L_α at $N_e=10^{17}$ cm^{-3} and $T=10^4$ K the simulation produces a line-center intensity which is 19% lower than a full MMM calculation and only 12% lower than a MMM profile using an impact theory with Greene's operator for the electrons. Thus the tendency of the full MMM is to produce less broadening in line center than the simulation, but the difference between the two is decreased if the MMM treatment of the electrons is replaced by an impact theory calculation.

The dip of L_β for H-Ar$^+$ case is again plotted in Fig. 13, as a function of density in the range 10^{15} cm$^{-3}<N_e<3.10^{17}$ cm^{-3}. For the high densities of the experiments both the simulation and MMM are close together and slightly higher than the experimental values. But again the functional dependence of the dip is better reproduced by the simulation calculation. Going toward lower densities, we observe an increasing discrepancy between the MMM and simulation. For $N_e=10^{15}$ cm^{-3}, the dip of the simulation has almost vanished, whereas the MMM predicts a dip still close to 0.25. At the present time it is not possible to compare the simulation and MMM to any L_β experimental data in this region of densities mainly because the profile is dominated by Doppler broadening. However, for H_β it was found that the experimental values fall considerably below the MMM as one goes to lower densities [see Fig. (1) of Ref. 32]. Thus one may expect the simulation to give better agreement with experimental data for the density dependence of the dip. It should be emphasized that the difference between the MMM and the simulation appears quite small when compared with the results of a static ion calculation which predicts a dip about four times larger at $N_e=10^{15}$ cm^{-3}.

Finally, in Fig. 14 we compare the half-width of L_α for the MMM and the simulation over the same density range. In the high-density region, the experimental points[33] are in good agreement with the simulation and deviate from the MMM by about 10%. The MMM half-width remains about (10—20)% below the simulation half-width for all densities plotted. We again note that the difference between the MMM and the simulation appears rather small when compared with a static ion calculation which is down by an order of magnitude at $N_e=10^{15}$ cm^{-3}.

To summarize the comparison with the MMM we may say that the two theories agree fairly well although the simulation predicts slightly more broadening or less structure in the line center which gives the simulation a slightly better agreement with experimental data. We have argued before[30] that the kangaroo process used by the MMM may be very useful in providing tractable analytic line-shape expressions but it does not seem to give a good

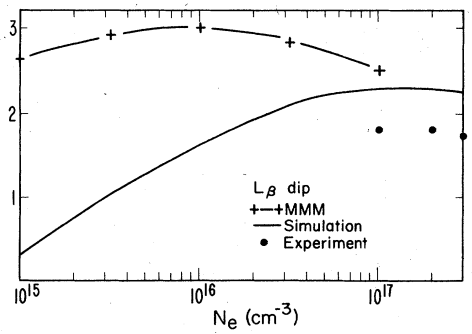

FIG. 13. L_β dip as a function of density for a fixed temperature $T=10\,000$ K. Theoretical MMM curves (Ref. 32) and simulation results are plotted for the density range 10^{15} cm$^{-3}<N_e<3\times10^{17}$ cm^{-3}. The experimental values (Ref. 33) correspond to the temperature range $12\,000\text{ K}<T<16\,000$ K.

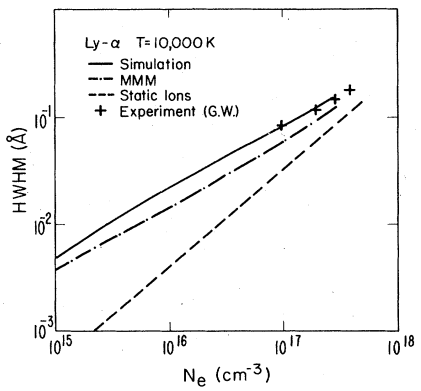

FIG. 14. Half-width at half maximum (HWHM) of L_α as a function of density for $T=10\,000$ K. Theoretical MMM curves (Ref. 32) and simulation results are plotted for the density range 10^{15} cm$^{-3}<N_e<3\times10^{17}$ cm^{-3}. The experimental values (Ref. 33) correspond to the temperature range $12\,000\text{ K}<T<16\,000$ K.

representation of the electric field fluctuations in a plasma. In a previous paper,[23] we pointed out that the conditional probability function obtained by computer simulation is not at all similar to the function obtained from a kangaroo process. This suggests that closer agreement between the MMM and the simulation might be obtained by improving the stochastic process used by the latter.

VI. CONCLUSIONS

In this paper we have presented a method for using a computer simulation of the ions in a plasma in the computation of spectral line profiles. The approximations that are used (e.g., Debye shielding, statistical independence of electrons and ions, etc.) are all thought to be accurate and are in fact commonly employed by most current theories. The advantage of the computer simulation is that it permits a calculation of dynamic ion effects without any new or unusual approximations.

In comparing the results of the computer simulation with experimental data, we obtain agreement to within 8% for the L_α half-width and 20% for the L_β dip at line center. For L_α, the agreement is comparable to the experimental error, which is the order of 5%, and it shows that essentially all of the previously observed discrepancies with static ion theories are due to ion dynamic effects. For L_β, ion dynamics reduced the dip from 0.41 to 0.25 but this is still 20% too large, hence there may still be some effects due to inelastic collisions, quadrupole interactions, etc. which need to be included. For L_γ and higher lines, ion dynamic effects are the order of 6% or less, and agreement with experimental data is within the experimental error.

We have also compared the computer simulation results with a new theory proposed by Greene[12] in which the electric fields are evaluated by following particle trajectories. In this comparison we found discrepancies the order of 25% to 30% which may result from the adiabatic approximation for the ion collision operator used by Greene.

Finally, we compared our results with the MMM, as developed by Seidel,[14,32] in which the electric fields are evaluated by means of a statistical model. In this case we found very close agreement within the temperature-density range of the experimental data. For L_α at $N_e = 10^{17}$ cm^{-3} and $T = 10^4$ K, the simulation produces a line-center intensity 19% below a full MMM calculation and only 12% below a calculation using the MMM for the ions and a time-ordered impact theory for the electrons. For L_β, the dip evaluated with the computer simulation has a significantly different density dependence from that predicted by the MMM with the discrepancy being greatest for low densities where ion dynamic effects are more important. Within the range of the L_β experimental data, the two calculations are quite close; however, an inference based on the density dependence of the H_β dip indicates that the simulation would give significantly better results for lower densities.

---

*Permanent address: Département de Physique des Interactions Ioniques et Moléculaires, Université de Provence, Centre Sainte Jérôme, F-13397 Marseille Cédex 13, France.

[1]K. Grützmacher and B. Wende, Phys. Rev. A **16**, 243 (1977).
[2]K. Grützmacher and B. Wende, Phys. Rev. A **18**, 2140 (1978).
[3]H. R. Griem, *Spectral Line Broadening by Plasmas* (Academic, New York, 1974).
[4]C. R. Vidal, J. Cooper, and E. W. Smith, Astrophys. J. Suppl. Ser. **25**, 37 (1973).
[5]W. L. Wiese, D. E. Kelleher, and D. R. Paquette, Phys. Rev. A **6**, 1132 (1972).
[6]D. E. Kelleher and W. L. Wiese, Phys. Rev. Lett. **31**, 1431 (1973).
[7]R. W. Lee, J. Phys. B **12**, 1145 (1979).
[8]H. R. Griem, Phys. Rev. A **20**, 606 (1979).
[9]D. Voslamber and R. Stamm, in *Spectral Line Shapes,* edited by B. Wende (de Gruyter, Berlin, 1981), p. 63.
[10]D. Voslamber, Z. Naturforsch. **24a**, 1458 (1969).
[11]E. W. Smith, J. Cooper, and C. R. Vidal, Phys. Rev. **185**, 140 (1969).
[12]R. Greene, J. Quant. Spectrosc. Radiat. Transfer **27**, 639 (1982).
[13]A. Brissaud and U. Frisch, J. Quant. Spectrosc. Radiat. Transfer **11**, 1767 (1971).
[14]J. Seidel, Z. Naturforsch. **32a**, 1207 (1977).
[15]W. R. Chappell, J. Cooper, and E. W. Smith, J. Quant. Spectrosc. Radiat. Transfer **10**, 1195 (1970).
[16]H. Capes and D. Voslamber, Phys. Rev. A **5**, 2528 (1972).
[17]H. Capes and D. Voslamber, Z. Naturforsch. **30a**, 913 (1975).
[18]P. Kepple and H. R. Griem, Phys. Rev. **173**, 317 (1968).
[19]S. T. Godfrey, C. R. Vidal, E. W. Smith, and J. Cooper, Phys. Rev. A **3**, 1543 (1971).
[20]We are grateful to R. Greene for providing us with a copy of his program.
[21]J. Seidel, Z. Naturforsch. **34a**, 1385 (1979).
[22]J. Seidel and R. Stamm, J. Quant. Spectrosc. Radiat. Transfer **27**, 499 (1982).
[23]E. W. Smith, R. Stamm, and J. Cooper (unpublished).
[24]R. Stamm and E. W. Smith (unpublished).
[25]International Mathematical and Statistical Library (Houston, Texas).
[26]C. F. Hooper, Phys. Rev. **165**, 215 (1968).
[27]M. Abramowitz and I. Stegun, *Handbook of Mathematical Functions,* Natl. Bur. Stand. (U.S.) Appl. Math. Ser. No. 55 (U.S. GPO, Washington, D.C., 1965).
[28]M. Geisler, K. Grützmacher, and B. Wende, in *Spectral Line Shapes II,* edited by Burnett (de Gruyter, Boulder, 1983), p. 37.
[29]M. Geisler, K. Grützmacher, and B. Wende, in *Spectral Line Shapes I,* edited by B. Wende (de Gruyter, Berlin, 1981), p. 103.
[30]E. W. Smith, B. Talin, and J. Cooper, J. Quant. Spectrosc. Radiat. Transfer **26**, 229 (1981).
[31]B. W. Shore and D. H. Menzel, *Principles of Atomic Spectra* (Wiley, New York, 1968).
[32]J. Seidel, in *Spectral Line Shapes,* edited by B. Wende (de Gruyter, Berlin, 1981), p. 3. Unpublished tables of MMM profiles calculated by J. Seidel are gratefully acknowledged.
[33]K. Grützmacher, Ph.D. dissertation, Technische Universität Berlin, 1979.